International Journal of Neural Systems, Vol. 18, No. 4 (2008) 267–277

World Scientific
www.worldscientific.com

EMERGENCE OF PREFERRED FIRING SEQUENCES IN LARGE SPIKING NEURAL NETWORKS DURING SIMULATED NEURONAL DEVELOPMENT

JAVIER IGLESIAS* and ALESSANDRO E. P. VILLA†
Grenoble Institut des Neurosciences — Equipe 7, Neuro-Heuristic Research Group
Université Joseph Fourier — Site Santé, Domaine de la Merci
F-38706 La Tronche cedex, France
**Javier.Iglesias@ujf-grenoble.fr*
†*Alessandro.Villa@ujf-grenoble.fr*

Two main processes concurrently refine the nervous system over the course of development: cell death and selective synaptic pruning. We simulated large spiking neural networks (100×100 neurons "at birth") characterized by an early developmental phase with cell death due to excessive firing rate, followed by the onset of spike timing dependent synaptic plasticity (STDP), driven by spatiotemporal patterns of stimulation. The cell death affected the inhibitory units more than the excitatory units during the early developmental phase. The network activity showed the appearance of recurrent spatiotemporal firing patterns along the STDP phase, thus suggesting the emergence of cell assemblies from the initially randomly connected networks. Some of these patterns were detected throughout the simulation despite the activity-driven network modifications while others disappeared.

Keywords: STDP; synaptic pruning; cell death; preferred firing sequences; cell assemblies.

1. Introduction

The adult pattern of neuronal connectivity in the cerebral cortex is determined by the expression of some genetic information and by epigenetic processes associated to plasticity and learning. During the early stages of development, excessive branches and synapses are initially formed and distributed somewhat diffusely.[1] This over-growth phase is generally followed by massive synaptic pruning[2] partially associated to genetically programmed cell death and pathologic or accidental cell death.

Quantitative analyses of synaptogenesis in the rat,[3] the Rhesus monkey,[4] and human cortex[5] have suggested a transient phase of high density of synapses during infancy. Over the course of development, complex connectivity patterns require the pruning of only a selected subset of the connections initially established by a neuron. Trigger signals able to induce selective synaptic pruning could be associated to patterns of activity that depend on the timing of action potentials.[6] Thus, the connectivity pattern of the cerebral cortex is completed by the time of sexual maturity as a result of the concurrent processes of cell death and selective axon pruning.

Spike timing dependent synaptic plasticity (STDP) is a change in the synaptic strength based on the ordering of pre- and post-synaptic spikes. It has been proposed as a mechanism to explain the origin of long-term potentiation (LTP), i.e. reinforcement of synapses repeatedly activated shortly before the occurrence of a post-synaptic spike.[7] STDP has also been proposed to explain long-term depression (LTD), the lasting weakening of synapses strength whenever the pre-synaptic cell is repeatedly activated shortly after the occurrence of a post-synaptic spike.[8] The study of the relation between synaptic efficacy and synaptic pruning suggests that the weak synapses may be modified and removed through competitive "learning" rules.[9] These mechanisms would contribute to maintain the average neuronal input to a post-synaptic neuron,[10] but would provoke

selective synaptic pruning in the sense that converging synapses are competing for control of the timing of post-synaptic action potentials.[11] Despite the plasticity of these phenomena it is rational to suppose that whenever the same information is presented in the network the same pattern of activity is evoked in a circuit of functionally interconnected neurons, referred to as "cell assembly". Cell assemblies interconnected in this way would be characterized by recurrent, above chance levels, ordered sequences of precise (in the order of few ms) interspike intervals referred to as spatiotemporal patterns of discharges or preferred firing sequences.[12] Such precise firing patterns have been associated with specific behavioral processes in rats[13] and primates.[14]

In the current study we introduce an "early developmental phase" characterized by cell death followed by the enabling of the synaptic modification rules applied to excitatory-excitatory (*exc*, *exc*) and excitatory-inhibitory (*exc*, *inh*) connections. We assume that developmental and/or learning processes are likely to potentiate or weaken certain pathways through the network and let emerge cell assemblies characterized by recurrent firing patterns. We investigate whether or not, and under which conditions, the dynamics of occurrence of spatiotemporal patterns of activity could be associated to emerging cell assemblies triggered by content-related stimuli organized in both temporal and spatial dimensions.

2. Methods

The originality of our study stands on the application of an original bio-inspired STDP modification rule compatible with hardware implementation.[15] The complete neural network model is described in details elsewhere.[16] A description of the model with specific model parameters related to the current study follows below.

2.1. *Neural network model*

We assume that at time zero of the simulation the network is characterized by two types of integrate-and-fire units and by its maximum over growth in terms of connectivity. The total amount of units is 10,000 (8,000 excitatory and 2,000 inhibitory) laid down on a 100×100 2D lattice according to a space-filling quasi-random Sobol distribution. Two sets of 400 excitatory units (i.e., 800 units overall), labeled sets A and B, were randomly selected among the 8,000 excitatory units of the network. The units belonging to sets A and B are the "sensory units" of the network, meaning that in addition to sending and receiving connections from the other units of both types they receive an input from the external stimulus.

All units of the network are simulated by leaky integrate-and-fire neuromimes. At each time step, the value of the membrane potential of the ith unit, $V_i(t)$, is calculated such that

$$\begin{aligned} V_i(t+1) = {} & V_{\mathrm{rest}[q]} + B_i(t) \\ & + (1 - S_i(t))((V_i(t) - V_{\mathrm{rest}[q]})k_{\mathrm{mem}[q]}) \\ & + \sum_j w_{ji}(t) \end{aligned}$$

where $V_{\mathrm{rest}}[q]$ corresponds to the value of the resting potential for the units of class type $[q]$, $B_i(t)$ is the background activity arriving to the ith unit, $S_i(t)$ is the state of the unit as expressed below, $k_{\mathrm{mem}}[q] = \exp(-1/\tau_{\mathrm{mem}}[q])$ is the constant associated to the current of leakage for the units of class type $[q]$, $w_{ji}(t)$ are the post-synaptic potentials of the jth units projecting to the ith unit.

The state of a unit $S_i(t)$ is a function of the membrane potential $V_i(t)$ and a threshold potential $\theta_{[q]_i}$, such that $S_i(t) = \mathcal{H}(V_i(t) - \theta_{[q]_i})$. $\mathcal{H}$ is the Heaviside function, $\mathcal{H}(x) = 0 : x < 0$, $\mathcal{H}(x) = 1 : x \geq 0$. It is assumed that a unit can generate a spike only for $S_i(t) = 1$. In addition, the state of the unit depends on the refractory period $t_{\mathrm{refract}}[q]$: after spiking, the membrane potential was reset to its resting potential, and the unit entered an absolute refractory period lasting 3 and 2 time steps for excitatory and inhibitory units, respectively. The relative refractory period was discarded from the model due to the restrictions imposed by the hardware implementation compatibility.

Sparse connections between the populations of units were randomly generated according to a 2D Gaussian density function with dense projections in a local neighborhood described elsewhere.[16] Long-range excitatory projections were allowed with a probability of 2%. Notice that edge effects induced by the borders were limited by folding the network as a torus.

The post-synaptic potential w_{ji} is a function of the state of the pre-synaptic unit S_j, of the type of

the synapse $P_{[q_j,q_i]}$, and of the activation level of the synapse A_{ji} discussed in the next section. This is expressed by the following equation

$$w_{ji}(t+1) = S_j(t) \cdot A_{ji}(t) \cdot P_{[q_j,q_i]}.$$

Notice that the type of the synapse is a parameter that depends on the types of units in the network. In the current study we assume that $P_{[1,1]}$, i.e. (exc, exc), and $P_{[1,2]}$ connections, i.e. (exc, inh), are of the same kind. The same assumption was made for $P_{[2,1]}$, i.e. (inh, exc), and $P_{[2,2]}$, i.e. (inh, inh) connections.

2.2. *Synaptic plasticity*

It is assumed *a priori* that modifiable synapses are characterized by discrete activation levels[17] that could be interpreted as a combination of two factors: the number of synaptic *boutons* between the pre- and post-synaptic units and the changes in synaptic conductance. In the current study we attributed a fixed activation level (meaning no synaptic modification) $A_{ji}(t) = 1$, to (*inh*, *exc*) and (*inh*, *inh*) synapses while activation levels were allowed to take one of $A_{ji}(t) = \{0, 1, 2, 4\}$ for (*exc, exc*) and (*exc*, *inh*), $A_{ji}(t) = 0$ meaning that the projection was permanently pruned out. For $A_{ji}(t) = 1$, the post-synaptic potentials were set to 0.84 mV and − 0.8 mV for excitatory and inhibitory units, respectively.

A *real-valued variable* $L_{ji}(t)$ is used to implement the spike-timing dependent plasticity rule for $A_{ji}(t)$, with integration of the timing of the pre- and post-synaptic activities. The variables $L_{ji}(t)$ are user-defined boundaries of attraction $L_0 < L_1 < L_2 < \cdots < L_{N-1} < L_N$ satisfying $L_{k-1} < [A_k] < L_k$ for $k = 1, \ldots, N$. This means that whenever $L_{ji} > L_k$ the activation variable A_{ji} jumps from state $[A_k]$ to $[A_{k+1}]$. Similarly, if $L_{ji} < L_k$ the activation variable A_{ji} jumps from state $[A_{k+1}]$ to $[A_k]$. Moreover, after a jump of activation level $[A]$ occurred at time t the real-valued variable L_{ij} is reset to $L_{ij}(t+1) = \frac{L_k + L_{k+1}}{2}$.

Spike-timing dependent plasticity (STDP) defines how the value of L_{ji} at time t is changed by the arrival of pre-synaptic spikes, by the generation of post-synaptic spikes and by the correlation existing between these events. On the generation of a post-synaptic spike (i.e., when $S_i = 1$), the value L_{ji} receives an *increment* which is a decreasing function of the elapsed time from the previous pre-synaptic spike at that synapse. Similarly, when a spike arrives at the synapse, the variable L_{ji} receives a *decrement* which is likewise a decreasing function of the elapsed time from the previous post-synaptic spike (i.e., when $S_j = 1$). This rule is summarized by the following equation: $L_{ji}(t+1) = L_{ji}(t) + (S_i(t) \cdot M_j(t)) - (S_j(t) \cdot M_i(t))$, where $S_i(t), S_j(t)$ are the state variables of the ith and jth units and $M_i(t), M_j(t)$ are interspike decay functions. $M_i(t)$ may be viewed as a "memory" of the latest interspike interval,

$$M_i(t+1) = S_i(t) M_{\max[q_i]} + (1 - S_i(t))(M_i(t) \exp(-t/\tau_{\text{syn}[q_i]}))$$

where $\tau_{\text{syn}}[q_i]$ is the synaptic plasticity time constant characteristic of each type of unit and $M_{\max}[q_i]$ was set $M_{\max}[q_i] = 2$ for all units of either type in this study. In the case that neither the pre- nor the post-synaptic unit is firing a spike, the real-valued variable will decay with a time constant $k_{\text{act}}[q_j, q_i] = \exp(-1/\tau_{\text{act}[q_j,q_i]})$ characteristic for each type of synapse, such that the final equation is the following:

$$L_{ji}(t+1) = L_{ji}(t) \cdot k_{\text{act}[q_j,q_i]} + (S_i(t) \cdot M_j(t)) - (S_j(t) \cdot M_i(t)).$$

2.3. *Cell death mechanisms*

The "death" of units is introduced in the current model and represents a major difference with our previous studies.[16] A dead unit is characterized by the absence of any spiking activity. Cell death may be provoked by two mechanisms: (i) an excessive firing rate and (ii) the loss of all excitatory inputs.

The glutamate is by far the main excitatory neurotransmitter in the cerebral cortex. An excessive firing rate is assumed to correspond to the biological effect known as glutamate neurotoxicity.[18] During an initial phase called "early developmental phase", at each time step and for each unit, an average firing rate $FR_{50}(i)$ is computed over a running window corresponding to 50 ms. For excitatory and inhibitory neurons a maximum firing rate *FRM* was arbitrarily determined following a parameter search procedure. In this study we used $FRM_{\text{exc}} = 245$ spikes/s and $FRM_{\text{inh}} = 250$ spikes/s respectively. If $FR_{50} > FRM$ for the corresponding unit type the cell had a probability to die according to the function

$$P_{\text{death}}(t) = \frac{0.5 \cdot t^2 - 4.5 \cdot 10^{-6} \cdot t^3}{44 \cdot (2.5 \cdot 10^6 + 6 \cdot 10^{-3} \cdot t^2)}. \quad (1)$$

with $P_{\text{death}}(t = 100\,\text{ms}) = 4.5 \cdot 10^{-5}$, $P_{\text{death}}(t = 700\,\text{ms}) = 2.2 \cdot 10^{-3}$, and $P_{\text{death}}(t = 80\,\text{ms}) = 2.9 \cdot 10^{-3}$. This function optimizes the number of units surviving the early developmental phase while maintaining a balanced excitatory/inhibitory ratio.

At the end of the early developmental phase, the synaptic plasticity is enabled.[19] The projections from and to "dead" units undergo a decay of their synapses leading eventually to their pruning when $A_{ji}(t) = 0$. Other projections may be pruned due to synaptic depression driven by STDP and also leading to $A_{ji}(t) = 0$. Thus, some units that survived the early phase can also remain without any excitatory input. The loss of all excitatory inputs provoke the cell death and these units stop firing (even in presence of background activity) immediately after the pruning of the last excitatory afference from within the network.

2.4. *Content-related stimuli*

Patterned activity organized both in time and space getting into the "sensory units" of the network is assumed to correspond to content-related activity generated elsewhere in the brain. Each stimulus lasted 100 ms and was followed by a period without stimulation that lasted 1900 ms. Thus, the rate of stimulation was 0.5 stim/s.

The spatial organization of the stimulus was determined by the following rules. The sets A and B of sensory units were divided into 10 groups of 40 units each, $A = \{A_1, A_2, \ldots, A_{10}\}$ and $B = \{B_1, B_2, \ldots, B_{10}\}$. During the first millisecond of the AB stimulation all 40 units belonging to the set A_1 received a large depolarization that induced a spike if the unit was not in a refractory period. At the next millisecond each unit belonging to the set A_2 was strongly activated and so forth until the units of set A_{10} were activated. The entire sequence of activation A_1A_{10} lasted 10 ms and was repeated 5 times, followed by 5 times the entire sequence B_1B_{10} (Fig. 1). A stimulus labeled BA was generated in a similar manner with 5 times the sequence B followed by 5 times the sequence A.

2.5. *Spike train analysis*

A spike train is composed by the time series of spike occurrences and is considered as a point process. The Poisson background noise alone can provoke a unit to fire whenever the excitability is close to the threshold of activation. Other spikes can be produced by the convergence of synchronous activity (i.e., temporal summation of excitatory post-synaptic potentials) generated within the network. In order to study the activity that is produced within the simulated network those spikes associated to the background process were recorded separately and discarded from the spike trains and the so-called "effective spike trains" are extracted.[20]

The effective spike trains were searched for the occurrence of spatiotemporal firing patterns. The pattern detection algorithm begins with finding all single or multineuron sequences of intervals that repeat two or more times within a record. Secondly, the algorithm computes how many of such sequences of intervals can be expected by chance and provides confidence limits for this estimation. The "pattern grouping algorithm"[21] performs clustering into one group of sequences of intervals with jitter in spike timing. Figure 2 illustrates the outline of this method. For the present study, the pattern grouping algorithm was used to find patterns of at least three spikes (triplets), with a minimal significance level of 10%, repeating at least 7 times in the interval [1–100] s, provided the entire pattern lasted not more than 800 ms and was repeated with an accuracy of ±5 ms.

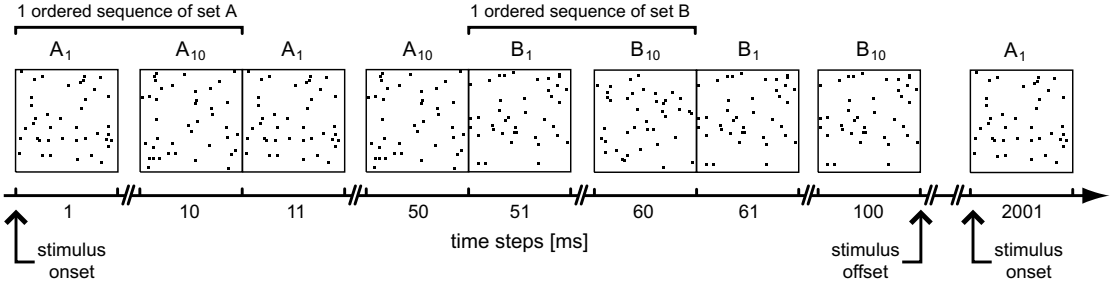

Fig. 1. Example of one AB stimulus presentation.

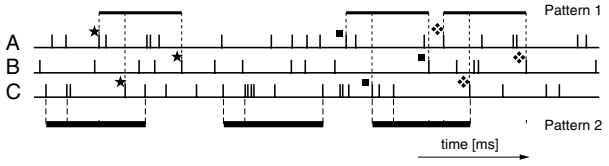

(a) Simultaneous recording of spike trains

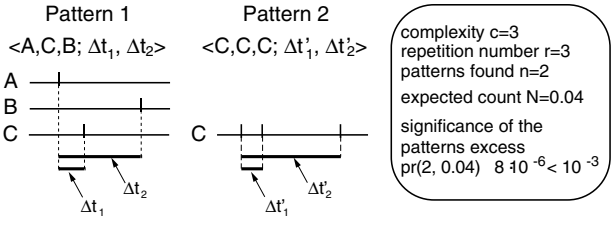

(b) Detection of statistically significant spatiotemporal firing patterns

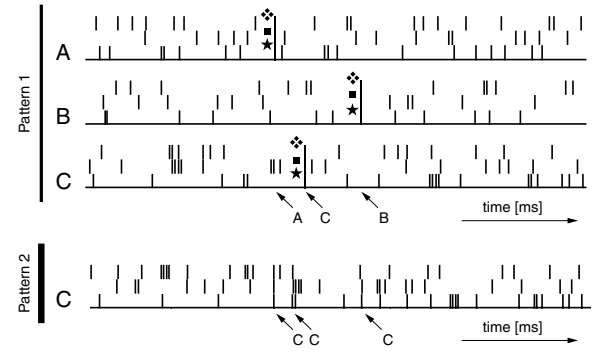

(c) Rasters of spikes aligned on pattern start

Fig. 2. Outline of the general procedure followed by pattern detection algorithms. (a): Analysis of a set of simultaneously recorded spike trains. Three cells, labeled A, B, and C, participate to a patterned activity. Three occurrences of two precise patterns are detected. Each occurrence of the pattern has been labeled by a specific marker in order to help the reader to identify the corresponding spikes. (b): Estimation of the statistical significance of the detected pattern. Two patterns, $n = 2$, $\langle \mathrm{A}, \mathrm{C}, \mathrm{B} \rangle$ and $\langle \mathrm{C}, \mathrm{C}, \mathrm{C} \rangle$ were found. Each pattern was formed by three neurons, $c = 3$, and was repeated three times, $r = 3$, in the analyzed record. The expected number of patterns of this complexity and repetition number was $N = 0.04$. The probability to observe 2 or more patterns when 0.04 patterns are expected is noted as $\mathrm{pr}\{2, 0.04\}$. (c): Display of pattern occurrences as a raster plot aligned on the pattern start.

3. Results

Each simulation run lasted 10^5 discrete time steps (T_{end}), with 1 time step corresponding to 1 ms in the model. The states (spiking/not spiking) of all units were updated synchronously. Starting at time zero and throughout all the simulation run each unit received a background activity following an independent Poisson process of 5 spikes/s on average.

The early developmental phase, characterized by cell death provoked by excessive firing rate, begins at time $t = 0$ and lasts until $t = T_{\mathrm{edp}}$. Two different early developmental phase durations have been investigated: $T_{\mathrm{edp}} = 700$ and $T_{\mathrm{edp}} = 800$. The spike timing dependent plasticity is enabled at $t = T_{\mathrm{edp}} + 1$. At time $t = 1001$ ms the first stimulation is applied, lasting 100 ms until $t = 1100$ ms. Between $t = 1101$ ms and $t = 2000$ ms only the background activity is getting into the network. At time $t = 2001$ ms another stimulation is applied and so forth until the end of the simulation run. Overall this corresponds to 50 presentations of the stimulus along one simulation run. The stimuli AB and BA appear in random order.

3.1. *Firing rate-induced cell death*

Figure 3 shows the evolution of the number of excitatory and inhibitory units during the first simulated second. For the first 800 time steps, units with mean firing rates exceeding the *FRM* threshold entered cell death with the probability expressed by $P_{\mathrm{death}}(t)$ (Eq. 1). The cell death dynamics was linearly fit with the probability function suggesting that the inhibitory units enter the cell death process about 70 ms before the excitatory units. At time $t = 1000$ ms, STDP-driven synaptic pruning could modify the synaptic weights, thus inducing cell death due to the loss of all excitatory inputs at a longer time-scale that is not depicted in Fig. 3.

The early developmental phase prevented the network from entering overactivity due to saturation by inducing the death of those units that tended to have an excessive activity since the early steps of the simulation. These units are known to destabilize the network and ignite the saturation.

In two different simulations, cell death was stopped after $T_{\mathrm{edp}} = 700$ ms or $T_{\mathrm{edp}} = 800$ ms time steps. With $T_{\mathrm{edp}} = 700$ ms, 956 excitatory units and 302 inhibitory units disappeared by $t = T_{\mathrm{edp}}$. With $T_{\mathrm{edp}} = 800$ ms, more time was allowed for "neurotoxic" cell death and 1355 excitatory units and 416 inhibitory units disappeared. Notice that the excitatory/inhibitory ratio changed from 4/1 at $t = 0$ to 4.15/1 and 4.19/1 with T_{edp} equal to 700 ms and 800 ms, respectively. The mean firing rate

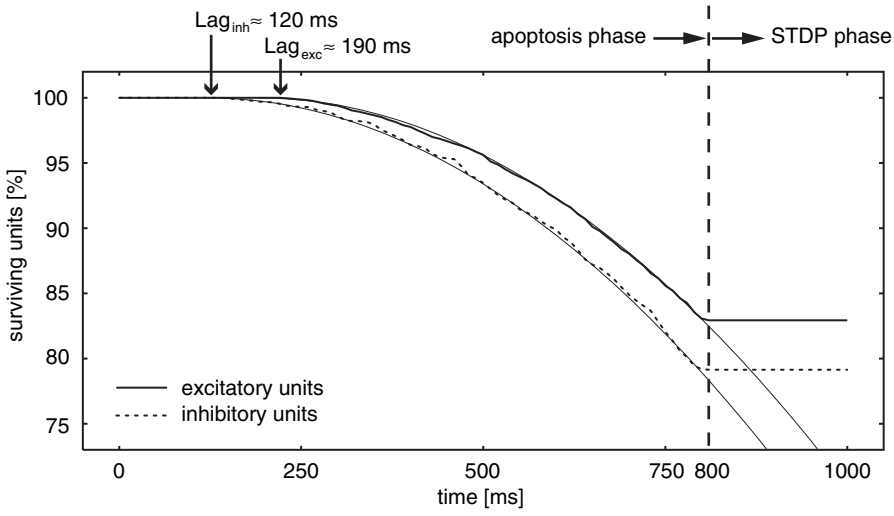

Fig. 3. Ratio of surviving units as a function of time with respect to initial conditions: 8000 excitatory units (plain line) and 2000 inhibitory units (dotted line). In this simulation, firing rate-induced cell death was stopped after 800 time steps ($T_{\rm edp} = 800$). Thin lines correspond to the fitting against the probability function $P_{\rm death}(t)$ with lags: 120 ms ($R^2 = 0.9797$) and 190 ms ($R^2 = 0.9902$) for the excitatory and inhibitory units, respectively.

of the excitatory units computed over the last second of simulation (i.e. just before $T_{\rm end}$) was 4.62 ± 3.41 spikes/s (average $\pm$ SD) with $T_{\rm edp} = 700$ ms, and 4.95 ± 3.96 spikes/s with $T_{\rm edp} = 800$ ms. In absence of early developmental phase, the mean firing rate computed over the last second of simulation was 4.32 ± 2.83 spikes/s. This indicates that less surviving units at $T_{\rm edp}$ can fire at higher rates.

3.2. *Spatiotemporal firing patterns*

One same network generated by the specified rules was simulated 5 times using 5 different random generator seeds, that produced 5 different spontaneous activity patterns. At time $t = T_{\rm end}$, the units, characterized by more than four active excitatory input projections that did not belong to the sets of stimulated units A or B, were selected and their effective spike trains were analyzed.

Among the 9 detected spatiotemporal firing patterns in these 5 simulations, three of them involving a single excitatory unit are detailed in the following paragraphs because they show representative features. Figures 4, 5 and 6 depict the results of their analysis.

The pattern $\langle$214F, 214F, 214F, 214F; 74 ± 4.5, 682 ± 2.5, $798 \pm 3.0\rangle$ was composed by spikes produced by a single unit labeled here #214F (Fig. 4a). This notation means that the pattern starts with a spike of unit #214F, followed 74 ± 4.5 ms by a second spike of the same unit, followed by a third spike 682 ± 2.5 ms after the first, and followed by a fourth spike 798 ± 3.0 ms after the first. Between $t = 1000$ ms and $t = T_{\rm end}$, 17 repetitions of the pattern were observed. The statistical significance of the excess of pattern occurrence computed by the pattern grouping algorithm[21] was $P = 3.9 \cdot 10^{-2}$. No correlation could be found between the timing of the spatiotemporal pattern and the stimulation onset (Fig. 4d). Figure 4e shows the occurrences of the pattern onset along the simulation time. The pattern occurred 1 time in the interval [1–25] s, 8 times in [25–50] s, and 8 times in [50–100] s. This might suggest that the network dynamics giving rise to the pattern appeared and was slowly disrupted by the continuous STDP-driven pruning. The distribution of pattern occurrences was tested against a linear regression with serial correlation between the residuals by the Durbin-Watson (DW) test[22,23] characterized by a statistic d and the sample size n. The value of d becomes smaller as the serial correlations increase. Figure 4f shows that the distribution of pattern occurrences is not regular. Indeed DW-test ($d = 0.4864$, $n = 17$) indicates successive error terms are, on average, positively correlated with significance $P \ll 1\%$.

The pattern $\langle$16A3, 16A3, 16A3; 274 ± 4.5, $708 \pm 1.5\rangle$ was composed by spikes produced by a single

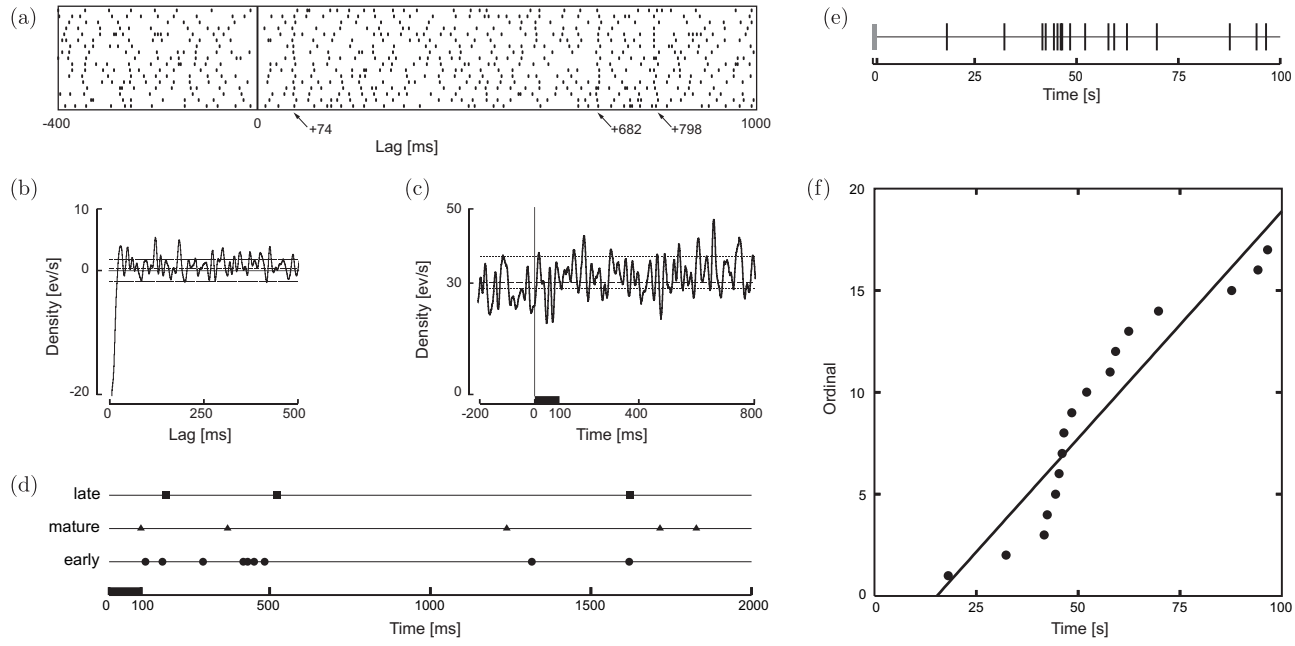

Fig. 4. Spatiotemporal pattern ⟨214F, 214F, 214F, 214F; 74 ± 4.5, 682 ± 2.5, 798 ± 3.0⟩. (a): Raster plot showing the 17 repetitions of the pattern aligned on the pattern start; (b): Autocorrelograms based on the differential time series recorded during the second preceding each stimuli onset showing no specifically correlated activity besides the absolute refractory period; (c): Peri-event density histogram lasting for 200 ms before to 800 ms after stimuli onset showing that the unit #214F activity is inhibited during stimulus presentation represented by the black line lasting 100 ms; (d): Pattern occurrence relative to stimulus presentation (black line lasting 100 ms) for the two seconds following stimulus onset during three arbitrary stages of the simulation: *early*: $1 \leq t < 50$ s; *mature*: $50 \leq t < 75$ s; *late*: $75 \leq t < 100$ s; (e): Pattern occurrence timing plot: each vertical tick represents the timing of the first pattern event; (f): Pattern occurrence regression plot: each black circle represents the timing of the first pattern event against its ordinal. The line represents the linear regression. It can be seen that the residuals of the regression, further investigated with the Durbin-Watson test, are serially correlated and not randomly distributed around the line.

unit labeled here #16A3 (Fig. 5a). The pattern was observed 41 times between $t = 1000$ ms and $t = T_{\text{end}}$ ($P = 4.2 \cdot 10^{-2}$). No correlation could be found between the timing of the spatiotemporal pattern and the stimulation onset (Fig. 5d). The pattern occurred 2 times in the interval [1–25] s, 10 times in [25–50] s, 17 times in [50–75] s, and 12 times in [75–100] s. This might suggest that the changes in the network dynamics induced by the continuous STDP-driven pruning lead to a transient state between [50–75] s seconds when the appearance of this pattern is favored. The linear regression on the pattern occurrence (Fig. 5f) is significant ($8.97 \cdot 10^{-32}$) and the Durbin-Watson test on the residuals ($d = 0.3884$, $n = 41$) indicates successive error terms are positively correlated ($P \ll 1\%$). Note that the pattern tends to occur in bursts.

The pattern ⟨BDC, BDC, BDC; 82 ± 3.5, 687 ± 5.5⟩ was composed by spikes produced by a single unit labeled here #BDC (Fig. 6a). In the interval [1–100] s, 56 repetitions of the pattern were observed ($P = 4.5 \cdot 10^{-5}$). Likewise the other firing patterns, no correlation could be found between the timing of the spatiotemporal pattern and the stimulation onset (Fig. 6d). The pattern occurred 12 times in the interval [1–50] s, 22 times in [50–75] s, and 22 times in [75–100] s. This might suggest that the network dynamics giving rise to the pattern was maintained for the last 50 seconds of simulation despite the continuous STDP-driven pruning. The linear regression on the pattern occurrence (Fig. 6f) is significant ($9.83 \cdot 10^{-42}$) and the Durbin-Watson test on the residuals ($d = 0.1376$, $n = 56$) indicates successive error terms are positively correlated ($P \ll 1\%$).

The down-pointing arrow on top of Fig. 6a indicates the timing of a putative fourth event being added to the triplet, about 300 ms before the first event of pattern ⟨BDC, BDC, BDC; 82 ± 3.5,

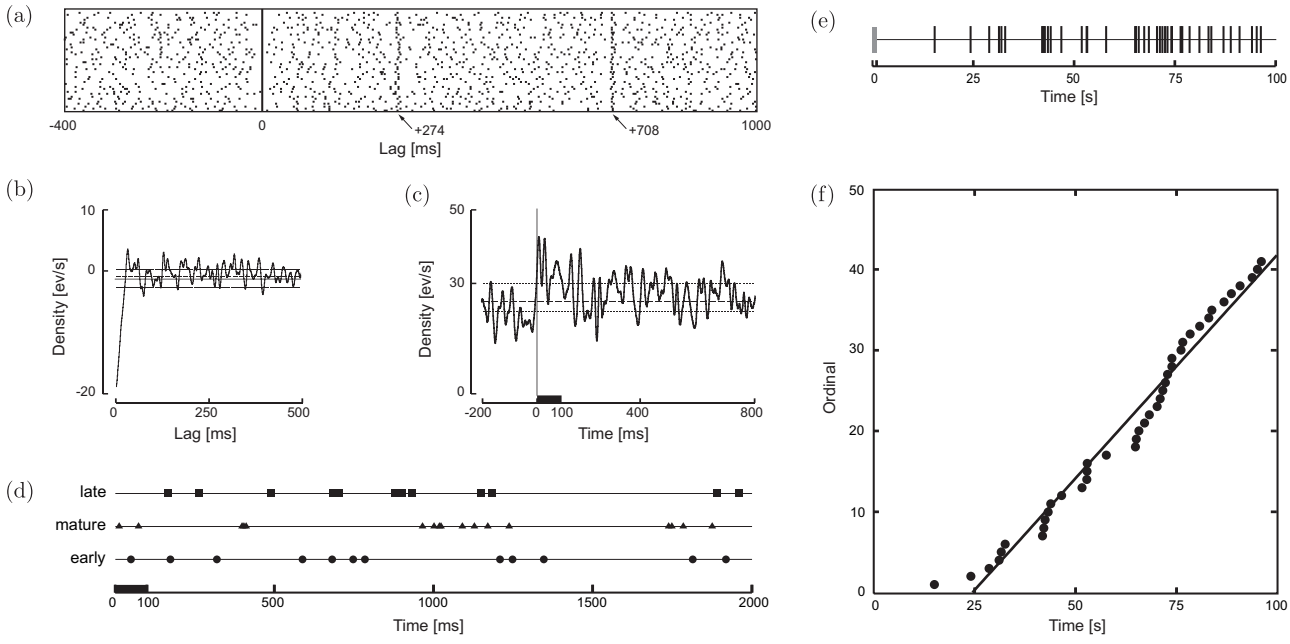

Fig. 5. Spatiotemporal pattern $\langle$16A3, 16A3, 16A3; 274 ± 4.5, $708 \pm 1.5\rangle$. (a): Raster plot showing the 41 repetitions of the pattern aligned on the pattern start; (b): Autocorrelograms based on the differential time series recorded during the second preceding each stimuli onset showing no specifically correlated activity besides the absolute refractory period; (c): Peri-event density histogram lasting for 200 ms before to 800 ms after stimuli onset showing that the unit #16A3 activity is larger during stimulus presentation represented by the black line lasting 100 ms; (d): Pattern occurrence relative to stimulus presentation (black line lasting 100 ms) for the two seconds following stimulus onset during three arbitrary stages of the simulation: *early*: $1 \leq t < 50$ s; *mature*: $50 \leq t < 75$ s; *late*: $75 \leq t < 100$ s; (e): Pattern occurrence timing plot: each vertical tick represents the timing of the first pattern event; (f): Pattern occurrence regression plot: each black circle represents the timing of the first pattern event against its ordinal. The line represents the linear regression. It can be seen that the residuals of the regression, further investigated with the Durbin-Watson test, are serially correlated and not randomly distributed around the line.

$687 \pm 5.5\rangle$. We observe that this additional event seems to "build up" a quadruplet during the simulation run, starting near $t = 60000$ ms (horizontal arrow on the raster display of Fig. 6a).

4. Discussion

We simulated a large scale spiking neural network, with the time resolution of 1 ms, characterized by a brief initial phase of cell death that extended our previous model.[16] The addition of this feature greatly improved the stability of the network while maintaining its ability to produce spatiotemporal firing patterns. During this phase the units that exceeded a certain threshold of firing had an increasing probability to die with the passing of time until 700 or 800 time units (depending on the simulation runs.) The inhibitory units entered the cell death process about 70 ms before the excitatory units. This delay is due to the build up of recurrent excessive excitation that affects in a different way the excitatory units (each one receiving, on average, 190 excitatory inputs and 460 inhibitory inputs) and the inhibitory units (each one receiving, on average, 90 excitatory inputs and 140 inhibitory inputs). The death dynamics of both populations followed the probability function to die with only minor deviations. After the stop of the massive cell death, spike timing dependent plasticity (STDP) and synaptic pruning were made active. Selected sets of units were activated by regular repetitions of a spatiotemporal pattern of stimulation. During the STDP phase, the cell death could occur only if a unit became deafferented, i.e. it lost all its excitatory afferences because of synaptic pruning.

We recorded the spike trains of all excitatory units that were not directly stimulated and that were surviving at the arbitrary end of the simulation set at $t = 10^5$ ms. In these spike trains we

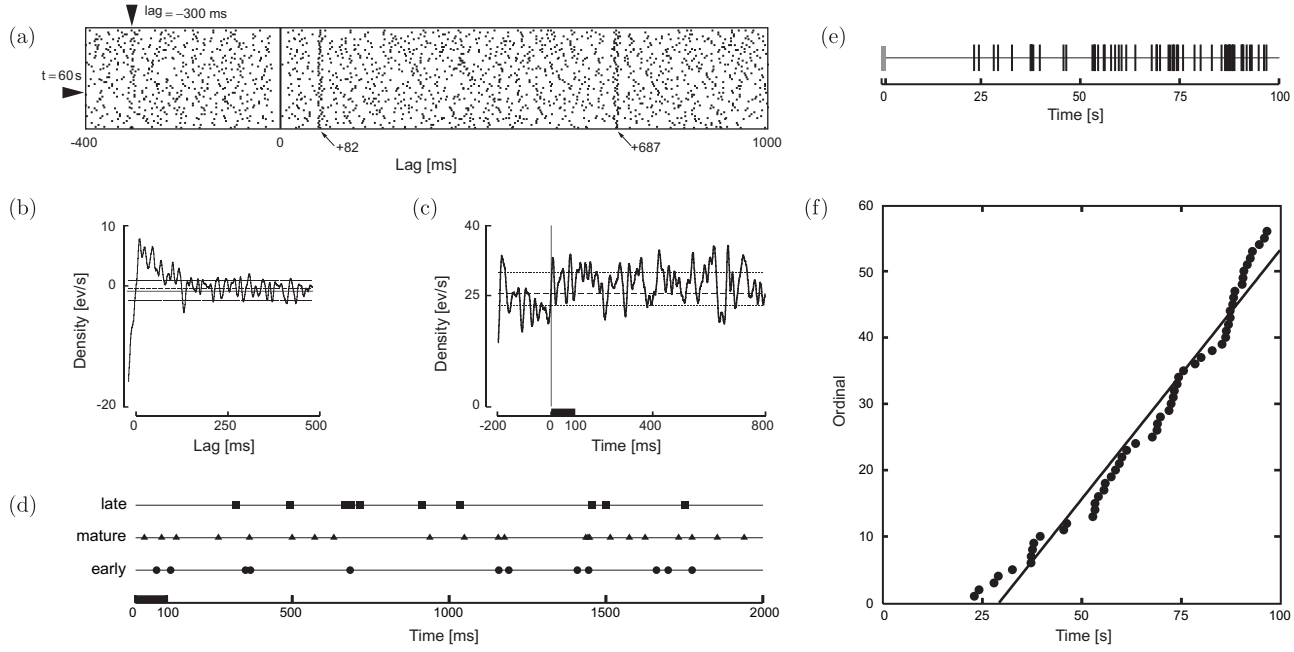

Fig. 6. Spatiotemporal pattern ⟨BDC, BDC, BDC; 82 ± 3.5, 687 ± 5.5⟩. (a): Raster plot showing the 56 repetitions of the pattern aligned on the pattern start; (b): Autocorrelograms based on the differential time series recorded during the second preceding each stimuli onset showing a positively correlated activity for short intervals besides from the absolute refractory period; (c): Peri-event density histogram lasting for 200 ms before to 800 ms after stimuli onset showing that the unit #BDC activity isn't affected by stimulus presentation represented by the black line lasting 100 ms; (d): Pattern occurrence relative to stimulus presentation (black line lasting 100 ms) for the two seconds following stimulus onset during three arbitrary stages of the simulation: *early*: $1 \leq t < 50$ s; *mature*: $50 \leq t < 75$ s; *late*: $75 \leq t < 100$ s; (e): Pattern occurrence timing plot: each vertical tick represents the timing of the first pattern event; (f): Pattern occurrence regression plot: each black circle represents the timing of the first pattern event against its ordinal. The line represents the linear regression. It can be seen that the residuals of the regression, further investigated with the Durbin-Watson test, are serially correlated and not randomly distributed around the line.

searched for preferred firing sequences that occurred beyond random expectation[21] and we found evidence of their appearance. We suggest that the detection of such preferred firing sequences might be associated with the emergence of cell assemblies from the initially locally connected random network.[19] This would be supported by the finding of the modifications induced by cell death and synaptic pruning in the subjacent network that lead to the appearance/disappearance of spatiotemporal patterns of activity. Figure 6a suggests that such modifications are part of a dynamical process that "builds up" as time runs and are therefor difficult to nail down.

The self-organization of spiking neurons into cell assemblies was reported in other studies of large simulated networks connected by STDP-driven projections.[24] These authors emphasized the emergence of spontaneously self-organized neuronal groups, even in absence of correlated input, associated with the spatiotemporal structure of firing patterns, if axonal conduction delays and STDP were incorporated in the model. They suggest these self-organizing groups generate stereotypical patterns of activity with millisecond precision through a mechanism called "polychronization".[25]

Our simulation results offer also the ground for testing several hypothesis with respect to neuroanatomical experimental results. Indeed, there is an increasing interest in investigating the cortical circuits and their synaptic connectivity with a statistical approach related to graph theory. Results obtained from layer 5 neurons in the visual cortex of developing rats[26] indicate that many aspects of the connectivity patterns differ from random networks. In particular, the distribution of synaptic connection strength in those cortical circuits show an overrepresentation of strong synaptic connections correlated with the overrepresentation of some connectivity

patterns. The authors[26] suggest that the local cortical network structure could be viewed as a skeleton of stronger connections in a sea of weaker ones.

The spike timing dependent plasticity rule implemented in our simulation has already been successfully implemented and tested in the POEtic tissue.[27] This electronic circuit is a flexible hardware substrate showing the basic features that permit living beings to show evolutionary, developmental or learning capabilities.[28] In future work, these features are intended to be implemented into a novel and even more flexible hardware architecture called *ubidule*[a]. The genomic features of these hardware tissues offer the possibility to implement programmed cell death mechanisms in simulations of large spiking neural networks. It is expected that the computational power of the dedicated platform will ease the simulation of larger networks to explore the impact of their size on the dynamics.

Acknowledgments

This work was partially funded by the European Community Future and Emerging Technologies Complex Systems program, grant #034632 (PERPLEXUS).

References

1. G. M. Innocenti, Exuberant development of connections, and its possible permissive role in cortical evolution, *Trends in Neurosciences* **18**(9) (1995) 397–402.
2. P. Rakic, J. P. Bourgeois, M. F. Eckenhoff, N. Zecevic and P. S. Goldman-Rakic, Concurrent overproduction of synapses in diverse regions of the primate cerebral cortex, *Science* **232** (1986) 232–235.
3. G. K. Aghajanian and F. E. Bloom, The formation of synaptic junctions in developing rat brain: A quantitative electron microscopic study, *Brain Research* **6**(4) (1967) 716–727.
4. J. Bourgeois and P. Rakic, Changes of synaptic density in the primary visual cortex of the macaque monkey from fetal to adult stage, *J. Neurosci.* **13** (1993) 2801–2820.
5. P. R. Huttenlocher, Synaptic density in human frontal cortex — Developmental changes and effects of aging, *Brain Research* **163**(2) (1979) 195–205.
6. S. M. Catalano and C.J. Shatz, Activity-dependent cortical target selection by thalamic axons, *Science* **281**(5376) (1998) 559–562.
7. C. C. Bell, V. Z. Han, Y. Sugawara and K. Grant, Synaptic plasticity in a cerebellum-like structure depends on temporal order, *Nature* **387**(6630) (1997) 278–281.
8. U. R. Karmarkar and D. V. Buonomano, A model of spike-timing dependent plasticity: One or two coincidence detectors?, *J. Neurophysiol.* **88** (2002) 507–513.
9. G. Chechik, I. Meilijson and E. Ruppin, Neuronal regulation: A mechanism for synaptic pruning during brain maturation, *Neural Computation* **11** (1999) 2061–2080.
10. S. Song and L. F. Abbott, Cortical development and remapping through spike timing-dependent plasticity, *Neuron* **32** (2001) 339–350.
11. R. Guyonneau, R. Van Rullen and S. J. Thorpe, Neurons tune to the earliest spikes through STDP, *Neural Computation* **17** (2005) 859–879.
12. M. Abeles, Corticonics: Neural circuits of the cerebral cortex, *Cambridge University Press* (1991).
13. A. E. P. Villa, I. Tetko, B. Hyland and A. Najem, Spatiotemporal activity patterns of rat cortical neurons predict responses in a conditioned task, *Proc. Natl. Acad. Sci. USA* **96** (1999) 1106–1111.
14. T. Shmiel, R. Drori, O. Shmiel, Y. Ben-Shaul, Z. Nadasdy, M. Shemesh, M. Teicher and M. Abeles, Temporally precise cortical firing patterns are associated with distinct action segments, *J. Neurophy.* **96**(5) (2006) 2645–2652.
15. J. Eriksson, O. Torres, A. Mitchell, G. Tucker, K. Lindsay, J. Rosenberg, J. M. Moreno and A. E. P. Villa, Spiking neural networks for reconfigurable POEtic tissue, *Lecture Notes in Computer Science* **2606** (2003) 165–174.
16. J. Iglesias, J. Eriksson, F. Grize, M. Tomassini and A. E. P. Villa, Dynamics of pruning in simulated large-scale spiking neural networks, *Biosystems* **79** (2005) 11–20.
17. J. M. Montgomery and D. V. Madison, Discrete synaptic states define a major mechanism of synapse plasticity, *Trends in Neurosciences* **27**(12) (2004) 744–750.
18. D. W. Choi, Glutamate neurotoxicity and diseases of the nervous system, *Neuron* **1**(8) (1988) 623–634.
19. J. Iglesias, J. Eriksson, B. Pardo, M. Tomassini and A. E. P. Villa, Stimulus-driven unsupervised pruning in large neural networks, *Lecture Notes in Computer Science* **3704** (2005) 59–68.
20. S. Hill and A. E. P. Villa, Dynamic transitions in global network activity influenced by the balance of excitation and inhibtion, *Network* **8** (1997) 165–184.
21. I. V. Tetko and A. E. P. Villa, A pattern grouping algorithm for analysis of spatiotemporal patterns in neuronal spike trains. 1. Detection of repeated patterns, *J. Neurosci. Meth.* **105** (2001) 1–114.

[a]http://www.perplexus.org/

22. J. Durbin and G. S. Watson, Testing for serial correlation in least squares regression. III, *Biometrika* **58**(1) (1971) 1–19.
23. N. R. Draper and H. Smith, Applied regression analysis (3rd ed.), *Wiley* (1998).
24. E. M. Izhikevich, J. A. Gally and G. M. Edelman, Spike-timing dynamics of neuronal groups, *Cerebral Cortex* **14** (2004) 933–944.
25. E. M. Izhikevich, Polychronization: Computation with spikes, *Neural Computation* **18** (2006) 245–282.
26. S. Song, P. J. Sjöström, M. Reigl, S. Nelson and D. B. Chklovskii, Highly nonrandom features of synaptic connectivity in local cortical circuits, *PLoS Biology* **3**(3) (2005) 0507–19.
27. J. M. Moreno, J. L. Eriksson, J. Iglesias and A. E. P. Villa, Implementation of biologically plausible spiking neural networks models on the POEtic tissue, *Lecture Notes in Computer Science* **3637** (2005) 188–197.
28. J. M. Moreno, Y. Thoma, E. Sanchez, J. Eriksson, J. Iglesias and A. E. P. Villa, The POEtic electronic tissue and its role in the emulation of large-scale biologically inspired spiking neural networks, *Complexus* **2006**(3) (2006) 32–47.